JOURNAL OF MOLECULAR SPECTROSCOPY 174, 253–269 (1995)

The High-Resolution Rotational–Torsional Spectrum of Methanol from 0.55 to 1.2 THz

S. P. BELOV,*[,1] G. WINNEWISSER,* AND ERIC HERBST†

*I. Physikalisches Institut, Universität zu Köln, D-50937 Cologne, Germany; and †Departments of Physics and Astronomy, Ohio State University, Columbus, Ohio 43210-1106

Received May 25, 1995; in revised form July 31, 1995

The rotational–torsional spectrum of gas-phase methanol (CH_3OH) has been studied at high resolution in the frequency range 0.55–1.2 THz. Over 450 new spectral lines belonging to 14 Q branches and 3 ^qR branches in the lowest three torsional states (v_t = 0–2) have been measured and analyzed. The lines have been added to previously measured transitions at lower frequency to comprise a global data set, which has been fit via an extended internal axis method in which transitions belonging to the A and E symmetry species are analyzed separately. © 1995 Academic Press, Inc.

I. INTRODUCTION

The rotational–torsional spectrum of gas-phase methanol remains an area of active interest to spectroscopists and astronomers. High-resolution measurements in the laboratory have now been undertaken at frequencies through 6 THz (*1*). Methanol is a well-known interstellar molecule, and copious transition frequencies have been detected in both quiescent and star-forming regions of interstellar clouds (*2*). For these latter regions, which are both warmer and denser than the ambient interstellar medium, transitions at frequencies approaching 1 THz and even higher are especially useful as probes of the physical conditions.

The spectrum of methanol is complicated by internal rotation, sometimes referred to as torsion, a large-amplitude motion in which the methyl protons rotate with respect to the hydroxyl portion of the molecule against a threefold symmetric potential (*3*). Internal rotation complicates the rotational spectrum of methanol in two ways. First, a number of torsional levels, characterized by the quantum number v_t = 0, 1, 2, · · · and the symmetry subclass (A or E), are thermally populated at room temperature so that rotational transitions within each of these torsional states are detectable. Second, internal rotation interacts with the end-over-end rigid body rotation of the molecule to produce a complex pattern which, especially for torsional levels of E symmetry, bears little resemblance to that of a normal asymmetric rotor. Two methods of analysis for this molecule have been utilized—the internal axis method (IAM), a quantum mechanical approach developed originally by Dennison and co-workers (*4*), and ex-

[1] On leave of absence from the Microwave Spectroscopy Laboratory, Institute of Applied Physics, Nizhnii Novgorod, Russia 603024.

0022-2852/95 $12.00

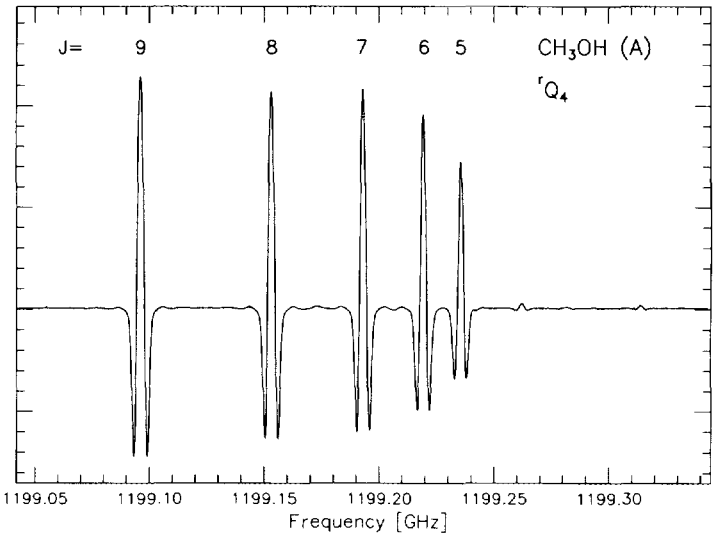

FIG. 1. The measured low J transitions constituting the head of the $^rQ_4$ ($\Delta J = 0$; $5 \leftarrow 4 = |K|$) branch of methanol in its ground torsional state of A symmetry are shown. The parity splittings are not resolved.

tended first by Lees and Baker (*3*) and subsequently by Herbst *et al.* (*5*) and De Lucia *et al.* (*6*), and a power series expansion for the energy levels, developed originally by Pickett *et al.* (*7*) and extended by Moruzzi and co-workers (*8*). The latter method

TABLE I

Newly Measured Q Branches

vt	A/E	K'	K"	Frequency (J_{min}) (GHz)	J_{max}
1	E	-7	-6	624.4	25
0	A	4	3	636.4 [a,b]	25
2	E	3	2	733.5	18
0	E	-5	-4	752.4	24
0	E	-3	-2	767.0	17
0	E	5	4	835.0	25
1	E	-2	-3	874.7	25
0	E	6	5	890.4 [c]	25
2	A	3	4	908.3 [b]	21
1	A	6	5	993.0 [b]	13
0	E	4	3	1006.1	23
1	E	-1	-2	1016.1	25
0	A	7	6	1062.0 [b]	25
0	A	5	4	1199.2	25

[a] Some lines previously measured in Ref. (*7*).
[b] Both parities measured; i.e., $- \leftarrow +$ and $+ \leftarrow -$.
[c] Some lines previously measured in Ref. (*23*).

TABLE II

CH_3OH *A* Transitions

v_t	J'	K'	P'	J"	K"	P"	Frequency (MHz)	Res. (MHz)	E_u (cm^{-1})	E_l (cm^{-1})	μ^2S
2	12	6	+	11	6	+	577466.585	-0.01	790.56	771.30	7.05
2	12	6	-	11	6	-	577466.585	-0.01	790.56	771.30	7.05
2	12	2	+	11	2	+	577551.585	-0.67	734.18	714.91	9.11
2	12	2	-	11	2	-	577551.585	-1.08	734.18	714.91	9.11
2	12	5	+	11	5	+	577666.814	0.05	729.80	710.53	7.77
2	12	5	-	11	5	-	577666.814	0.05	729.80	710.53	7.77
1	12	6	+	11	6	+	577808.552	-0.02	450.77	431.50	7.05
1	12	6	-	11	6	-	577808.552	-0.02	450.77	431.50	7.05
1	12	1	+	11	1	+	577903.803	-0.08	351.41	332.13	9.31
2	12	3	+	11	3	+	577939.758	0.19	582.49	563.21	8.80
2	12	3	-	11	3	-	577939.758	0.21	582.49	563.21	8.80
2	12	4	+	11	4	+	577970.713	0.18	552.20	532.92	8.44
2	12	4	-	11	4	-	577970.713	0.18	552.20	532.92	8.44
2	12	0	+	11	0	+	577996.382	0.40	478.35	459.07	9.40
1	12	9	+	11	9	+	578250.702	0.00	600.48	581.19	4.11
1	12	9	-	11	9	-	578250.702	0.00	600.48	581.19	4.11
1	12	7	+	11	7	+	578341.346	-0.20	563.11	543.82	6.20
1	12	7	-	11	7	-	578341.346	-0.20	563.11	543.82	6.20
1	12	5	+	11	5	+	578387.221	-0.05	417.71	398.42	7.77
1	12	5	-	11	5	-	578387.221	-0.05	417.71	398.42	7.77
1	12	2	+	11	2	+	578487.012	0.09	333.05	313.76	9.17
1	12	2	-	11	2	-	578537.919	0.04	333.06	313.76	9.17
1	12	3	+	11	3	+	578685.314	0.25	400.78	381.48	8.82
1	12	3	-	11	3	-	578685.314	-0.32	400.78	381.48	8.82
1	12	0	+	11	0	+	578820.112	-0.17	420.02	400.71	9.40
2	12	1	-	11	1	-	578999.743	0.14	599.88	580.57	9.33
1	12	1	-	11	1	-	579048.366	0.00	351.65	332.34	9.31
1	12	4	+	11	4	+	579123.010	0.47	459.86	440.55	8.22
1	12	4	-	11	4	-	579123.010	0.47	459.86	440.55	8.22
0	12	0	+	11	0	+	579459.632	-0.04	125.74	106.41	9.40
0	12	8	+	11	8	+	579722.453	-0.13	348.81	329.47	5.22
0	12	8	-	11	8	-	579722.453	-0.13	348.81	329.47	5.22
0	12	7	+	11	7	+	579792.180	0.07	295.82	276.48	6.20
0	12	7	-	11	7	-	579792.180	0.07	295.82	276.48	6.20
0	12	2	-	11	2	-	579858.245	-0.02	152.00	132.66	9.20
0	12	6	+	11	6	+	579932.695	0.08	260.42	241.08	7.05
0	12	6	-	11	6	-	579932.695	0.08	260.42	241.08	7.05
0	12	5	+	11	5	+	580058.360	0.08	221.64	202.29	7.82
0	12	5	-	11	5	-	580058.360	0.08	221.64	202.29	7.82
0	12	3	+	11	3	+	580175.969	-0.02	160.43	141.08	8.79
0	12	4	+	11	4	+	580195.213	-0.35	181.66	162.30	8.38

[a] Remeasurement of lines originally measured by Pickett *et al.* (*7*) not included in previous fits.

[b] Remeasurement of lines originally measured by Pickett *et al.* (*7*) and included in previous fits.

has proven to be especially useful for assigning both rotational and torsional transitions in the far-infrared (*1*).

The most recent IAM treatments of the high-resolution rotational spectrum are those of Anderson *et al.* (*9*) and Xu and Hougen (*10*). Anderson *et al.* included 1073 transitions mainly under 600 GHz in frequency, most of which had been checked carefully by loop and/or "error-curve" analyses. The error-curve technique relies on the smooth variation with rotational quantum number J of the difference between observed and calculated transition frequencies in a given family. Anderson *et al.* analyzed transitions in the lowest three torsional states

TABLE II—*Continued*

v_t	J'	K'	P'	J"	K"	P"	Frequency (MHz)	Res. (MHz)	E_u (cm^{-1})	E_l (cm^{-1})	μ^2S	
0	12	4	-	11	4	-	580195.213	0.31	181.66	162.30	8.38	
0	12	3	-	11	3	-	580212.776	-0.01	160.43	141.08	8.79	
0	12	2	+	11	2	+	580501.973	-0.02	152.07	132.71	9.20	
0	25	4	+	25	3	-	635670.305	0.21	579.80	558.60	28.54	
0	24	4	+	24	3	-	635872.128	-0.01	539.52	518.31	27.10	
0	23	4	+	23	3	-	636012.281	-0.12	500.85	479.64	25.70	
0	22	4	+	22	3	-	636104.302	-0.18	463.79	442.57	24.34	
0	21	4	+	21	3	-	636160.037	-0.20	428.33	407.11	23.00	
0	14	4	+	14	3	-	636190.130	-0.86	225.20	203.98	14.27	
0	15	4	+	15	3	-	636190.130	-0.06	249.39	228.16	15.46	
0	20	4	+	20	3	-	636190.130	0.33	394.48	373.26	21.68	
0	16	4	+	16	3	-	636193.310	-0.11	275.18	253.96	16.67	
0	13	4	+	13	3	-	636196.843	-0.16	202.62	181.40	13.08	
0	17	4	+	17	3	-	636198.580	-0.05	302.59	281.37	17.89	
0	19	4	+	19	3	-	636201.600	-0.08	362.24	341.02	20.40	
0	18	4	+	18	3	-	636202.520	-0.26	331.61	310.39	19.13	
0	12	4	+	12	3	-	636208.620	-0.06	181.66	160.43	11.91	
0	11	4	+	11	3	-	636225.853	-0.04	162.30	141.08	10.74	
0	10	4	+	10	3	-	636248.024	-0.03	144.56	123.34	9.56	
0	9	4	+	9	3	-	636274.190	-0.01	128.43	107.21	8.38	a
0	10	4	-	10	3	+	636279.380	0.03	144.56	123.34	9.56	a
0	11	4	-	11	3	+	636280.420	-0.10	162.30	141.08	10.73	
0	9	4	-	9	3	+	636291.094	-0.01	128.43	107.21	8.38	b
0	12	4	-	12	3	+	636299.400	-0.03	181.66	160.43	11.91	
0	8	4	+	8	3	-	636303.169	0.01	113.92	92.69	7.18	b
0	8	4	-	8	3	+	636311.642	0.01	113.92	92.69	7.18	b
0	7	4	+	7	3	-	636333.628	0.03	101.01	79.79	5.96	b
0	7	4	-	7	3	+	636337.460	0.01	101.01	79.79	5.96	b
0	13	4	-	13	3	+	636341.675	-0.03	202.62	181.40	13.08	
0	6	4	+	6	3	-	636364.090	-0.01	89.72	68.49	4.68	b
0	6	4	-	6	3	+	636365.730	0.08	89.72	68.49	4.68	a
0	5	4	+	5	3	-	636393.608	0.31	80.04	58.81	3.32	a
0	5	4	-	5	3	+	636393.608	-0.20	80.04	58.81	3.32	a
0	14	4	-	14	3	+	636413.741	-0.02	225.20	203.97	14.26	
0	4	4	+	4	3	-	636420.012	0.14	71.98	50.75	1.81	a
0	4	4	-	4	3	+	636420.012	0.01	71.98	50.75	1.81	a
0	15	4	-	15	3	+	636522.966	0.02	249.39	228.15	15.45	
0	17	4	-	17	3	+	636886.939	0.09	302.59	281.35	17.87	
0	18	4	-	18	3	+	637161.287	0.13	331.61	310.36	19.10	
0	18	0	+	17	0	+	867326.686	-0.29	275.35	246.42	14.09	
1	18	3	+	17	3	+	867590.584	-0.01	550.34	521.40	13.72	
1	18	3	-	17	3	-	867595.003	0.13	550.34	521.40	13.72	
1	18	1	-	17	1	-	867643.102	-0.21	501.25	472.31	14.02	
1	18	0	+	17	0	+	867722.988	-0.34	569.60	540.66	14.09	

through rotational quantum numbers $J = 24$ and $K = 7$. Considering the transitions in the A and E torsional substates separately, they were able to fit the transitions with variances of 86 kHz (A) and 83 kHz (E) by varying 57 and 64 parameters, respectively. The parameters, or "spectroscopic constants," used multiply rotational, torsional, and torsional–rotational ("interaction") operator expressions in a rather large Hamiltonian (*9*).

Xu and Hougen (*10*) carried out a global fit of 730 "microwave" transitions of the $v_t = 0$ state in both symmetry classes involving $J \leqslant 20$, $K \leqslant 12$ and 1320 Fourier-transform far-infrared transitions by varying 43 parameters. About 100 newly measured high-resolution far-infrared lines obtained by Matsushima *et al.* (*11*) at frequencies exceeding 1.5 THz were also included in a late stage of the work. The high-resolution lines were fit to experimental accuracy ($\approx$50 kHz) as long as the K values were kept below an upper limit ($K \leqslant 12$). Xu and Hougen

TABLE II—*Continued*

v_t	J'	K'	P'	J"	K"	P"	Frequency (MHz)	Res. (MHz)	E_u (cm^{-1})	E_l (cm^{-1})	μ^2S
0	18	2	-	17	2	-	868517.932	-0.10	301.77	272.80	14.01
0	18	8	+	17	8	+	868971.169	-0.02	498.61	469.63	11.31
0	18	8	-	17	8	-	868971.169	-0.02	498.61	469.63	11.31
0	18	7	+	17	7	+	869000.192	0.09	445.64	416.65	11.97
0	18	7	-	17	7	-	869000.192	0.09	445.64	416.65	11.97
0	18	6	+	17	6	+	869175.907	0.08	410.27	381.27	12.52
0	18	6	-	17	6	-	869175.907	0.08	410.27	381.27	12.52
0	18	5	+	17	5	+	869506.745	0.01	371.54	342.53	13.09
0	18	5	-	17	5	-	869506.745	-0.05	371.54	342.53	13.09
0	18	3	+	17	3	+	869691.326	-0.07	310.36	281.35	13.68
0	18	4	-	17	4	-	869965.676	-0.03	331.61	302.59	13.43
0	18	3	-	17	3	-	869973.368	-0.01	310.39	281.37	13.68
0	18	4	+	17	4	+	869977.511	-0.03	331.61	302.59	13.43
2	21	3	-	21	4	+	907845.180	-0.13	828.13	797.85	4.46
2	21	3	+	21	4	-	907846.760	-0.10	828.13	797.85	4.46
2	20	3	+	20	4	-	907868.215	-0.57	794.43	764.15	4.26
2	20	3	-	20	4	+	907868.215	0.57	794.43	764.15	4.26
2	19	3	+	19	4	-	907893.708	-0.34	762.33	732.05	4.06
2	19	3	-	19	4	+	907893.708	0.50	762.33	732.05	4.06
2	18	3	+	18	4	-	907921.758	-0.19	731.84	701.55	3.85
2	18	3	-	18	4	+	907921.758	0.41	731.84	701.55	3.85
2	17	3	+	17	4	-	907951.761	-0.10	702.94	672.65	3.65
2	17	3	-	17	4	+	907951.761	0.32	702.94	672.65	3.65
2	16	3	+	16	4	-	907983.143	-0.04	675.64	645.36	3.43
2	16	3	-	16	4	+	907983.143	0.24	675.64	645.36	3.43
2	15	3	+	15	4	-	908015.369	-0.02	649.95	619.66	3.22
2	15	3	-	15	4	+	908015.369	0.17	649.95	619.66	3.22
2	14	3	+	14	4	-	908047.942	-0.01	625.86	595.57	3.00
2	14	3	-	14	4	+	908047.942	0.12	625.86	595.57	3.00
2	13	3	+	13	4	-	908080.398	-0.01	603.37	573.08	2.77
2	13	3	-	13	4	+	908080.398	0.07	603.37	573.08	2.77
2	12	3	+	12	4	-	908112.303	-0.01	582.49	552.20	2.55
2	12	3	-	12	4	+	908112.303	0.04	582.49	552.20	2.55
2	11	3	+	11	4	-	908143.264	-0.02	563.21	532.92	2.31
2	11	3	-	11	4	+	908143.264	0.01	563.21	532.92	2.31
2	10	3	+	10	4	-	908172.917	-0.02	545.54	515.25	2.07
2	10	3	-	10	4	+	908172.917	0.00	545.54	515.25	2.07
2	9	3	+	9	4	-	908200.927	-0.02	529.47	499.18	1.83
2	9	3	-	9	4	+	908200.927	-0.01	529.47	499.18	1.83
2	8	3	+	8	4	-	908226.988	-0.02	515.01	484.71	1.60
2	8	3	-	8	4	+	908226.988	-0.02	515.01	484.71	1.60
2	7	3	+	7	4	-	908250.851	0.00	502.15	471.86	1.33
2	7	3	-	7	4	+	908250.851	0.00	502.15	471.86	1.33
2	6	3	+	6	4	-	908272.234	-0.01	490.90	460.61	1.05

argued that the high-K limitation of the model in the $v_t = 0$ level is caused by interactions with low-K $v_t = 1$ rotational–torsional levels, although the extended IAM treatment contains matrix elements for the interactions of levels of differing torsional quantum number. Xu and Hougen have recently extended their analysis to include transitions involving the $v_t = 1$ torsional level (*12*).

In addition to these two approaches, Tsunekawa *et al.* (*13*) have recently assigned 934 of 5000 lines in the region 7–200 GHz and have reanalyzed the spectrum using a reduced IAM Hamiltonian (*14*) including only experimentally determinable parameters through eighth order.

The list of analyzed high-resolution rotational–torsional transitions in methanol includes very few lines at frequencies between 500 and 1500 GHz (*1*). This effective gap in the spectrum of methanol and other molecules can now be closed by use of high-frequency backward-wave oscillators (BWOs) as sources of radia-

TABLE II—*Continued*

v_t	J'	K'	P'	J"	K"	P"	Frequency (MHz)	Res. (MHz)	E_u (cm^{-1})	E_l (cm^{-1})	$\mu^2 S$
2	6	3	-	6	4	+	908272.234	-0.01	490.90	460.61	1.05
2	5	3	+	5	4	-	908290.966	0.01	481.26	450.96	0.75
2	5	3	-	5	4	+	908290.966	0.01	481.26	450.96	0.75
2	4	3	+	4	4	-	908306.845	0.01	473.23	442.93	0.41
2	4	3	-	4	4	+	908306.845	0.01	473.23	442.93	0.41
1	13	6	+	13	5	-	990518.360	-0.02	471.65	438.61	10.02
1	13	6	-	13	5	+	990518.360	-0.02	471.65	438.61	10.02
1	12	6	+	12	5	-	991265.678	-0.01	450.77	417.71	8.97
1	12	6	-	12	5	+	991265.678	-0.01	450.77	417.71	8.97
1	11	6	+	11	5	-	991844.347	-0.04	431.50	398.42	7.90
1	11	6	-	11	5	+	991844.347	-0.04	431.50	398.42	7.90
1	10	6	+	10	5	-	992279.482	-0.06	413.83	380.73	6.79
1	10	6	-	10	5	+	992279.482	-0.06	413.83	380.73	6.79
1	9	6	+	9	5	-	992594.919	-0.05	397.76	364.65	5.63
1	9	6	-	9	5	+	992594.919	-0.05	397.76	364.65	5.63
1	8	6	+	8	5	-	992812.907	-0.03	383.29	350.17	4.41
1	8	6	-	8	5	+	992812.907	-0.03	383.29	350.17	4.41
1	7	6	+	7	5	-	992953.880	0.03	370.43	337.31	3.10
1	7	6	-	7	5	+	992953.880	0.03	370.43	337.31	3.10
1	6	6	+	6	5	-	993036.250	0.10	359.17	326.05	1.65
1	6	6	-	6	5	+	993036.250	0.10	359.17	326.05	1.65
1	22	1	+	21	1	+	1057402.959	0.15	632.22	596.95	17.16
0	22	0	+	21	0	+	1058124.662	-0.11	406.99	371.70	17.22
1	22	2	+	21	2	+	1058598.633	-0.28	614.17	578.86	17.13
0	25	7	+	25	6	-	1059188.264	-0.17	693.45	658.12	22.97
0	25	7	-	25	6	+	1059188.264	-0.10	693.45	658.12	22.97
0	24	7	+	24	6	-	1059350.625	-0.04	653.24	617.91	21.93
0	24	7	-	24	6	+	1059350.625	0.00	653.24	617.91	21.93
1	22	1	-	21	1	-	1059446.968	0.08	633.02	597.68	17.15
0	23	7	+	23	6	-	1059519.321	0.04	614.64	579.29	19.08
0	23	7	-	23	6	+	1059519.321	0.06	614.64	579.29	19.08
0	22	7	+	22	6	-	1059692.740	0.07	577.63	542.28	18.28
0	22	7	-	22	6	+	1059692.740	0.08	577.63	542.28	18.28
0	21	7	+	21	6	-	1059869.323	0.03	542.23	506.87	17.46
0	21	7	-	21	6	+	1059869.323	0.04	542.23	506.87	17.46
1	22	3	+	21	3	+	1059907.875	-0.16	682.14	646.78	16.92
1	22	3	-	21	3	-	1059919.402	0.08	682.14	646.78	16.92
1	22	0	+	21	0	+	1059996.668	0.11	701.41	666.06	17.22
0	20	7	+	20	6	-	1060047.757	0.06	508.43	473.07	16.60
0	20	7	-	20	6	+	1060047.757	0.06	508.43	473.07	16.60
0	22	2	-	21	2	-	1060160.286	0.26	433.64	398.28	17.18
0	19	7	+	19	6	-	1060226.537	0.04	476.23	440.86	15.71
0	19	7	-	19	6	+	1060226.537	0.04	476.23	440.86	15.71
0	18	7	+	18	6	-	1060404.402	0.02	445.64	410.27	14.79

tion. These BWOs with support electronics have been installed in Cologne (*15*). In this paper, we report the measurement and analysis of approximately 480 newly studied rotational–torsional transitions of methanol in the frequency range 0.55–1.2 THz through $J = 25$. The transitions belong to 14 Q branches ($\Delta J = 0$, $\Delta K = \pm 1$), 12 of which have been studied for the first time, as well as 3 new ^qR branches ($\Delta J = 1$, $\Delta K = 0$) in the torsional states $v_t = 0, 1, 2$. The transitions have been added to the data set of Anderson *et al.* (*9*) and fit using the IAM approach.

II. EXPERIMENTAL AND THEORETICAL

High-resolution spectral measurements in the region 0.55–1.2 THz have been undertaken with BWOs (ISTOK Research and Production Co., Fryazino, Russia)

TABLE II—*Continued*

v_t	J'	K'	P'	J"	K"	P"	Frequency (MHz)	Res. (MHz)	E_u (cm^{-1})	E_l (cm^{-1})	μ^2S
0	18	7	-	18	6	+	1060404.402	0.02	445.64	410.27	14.79
0	17	7	+	17	6	-	1060580.118	0.00	416.65	381.27	13.84
0	17	7	-	17	6	+	1060580.118	0.00	416.65	381.27	13.84
0	16	7	+	16	6	-	1060752.507	-0.01	389.27	353.89	13.43
0	16	7	-	16	6	+	1060752.507	-0.01	389.27	353.89	13.43
0	15	7	+	15	6	-	1060920.465	-0.02	363.50	328.11	12.30
0	15	7	-	15	6	+	1060920.465	-0.02	363.50	328.11	12.30
0	14	7	+	14	6	-	1061082.902	-0.08	339.33	303.94	11.16
0	14	7	-	14	6	+	1061082.902	-0.08	339.33	303.94	11.16
0	13	7	+	13	6	-	1061239.012	-0.02	316.77	281.37	9.99
0	13	7	-	13	6	+	1061239.012	-0.02	316.77	281.37	9.99
0	12	7	+	12	6	-	1061387.721	-0.01	295.82	260.42	8.79
0	12	7	-	12	6	+	1061387.721	-0.01	295.82	260.42	8.79
0	22	8	+	21	8	+	1061409.897	0.08	630.61	595.20	14.95
0	22	8	-	21	8	-	1061409.897	0.08	630.61	595.20	14.95
0	11	7	+	11	6	-	1061528.233	0.00	276.48	241.08	7.54
0	11	7	-	11	6	+	1061528.233	0.00	276.48	241.08	7.54
0	22	6	+	21	6	+	1061539.844	-0.01	542.28	506.87	15.94
0	22	6	-	21	6	-	1061539.844	0.00	542.28	506.87	15.94
0	10	7	+	10	6	-	1061659.539	-0.23	258.75	223.34	6.25
0	10	7	-	10	6	+	1061659.539	-0.23	258.75	223.34	6.25
0	9	7	+	9	6	-	1061781.646	0.03	242.63	207.22	4.88
0	9	7	-	9	6	+	1061781.646	0.03	242.63	207.22	4.88
0	8	7	+	8	6	-	1061893.181	0.05	228.13	192.70	3.41
0	8	7	-	8	6	+	1061893.181	0.05	228.13	192.70	3.41
0	7	7	+	7	6	-	1061993.806	0.08	215.23	179.80	1.80
0	7	7	-	7	6	+	1061993.806	0.08	215.23	179.80	1.80
0	22	5	+	21	5	+	1062098.053	0.20	503.62	468.19	16.44
0	22	5	-	21	5	-	1062098.053	-0.21	503.62	468.19	16.44
0	22	3	+	21	3	+	1062261.797	0.11	442.46	407.03	16.88
0	22	4	-	21	4	-	1062920.494	0.02	463.78	428.32	16.70
0	22	4	+	21	4	+	1062968.488	0.02	463.79	428.33	16.70
0	22	3	-	21	3	-	1063024.214	-0.01	442.57	407.11	16.88
0	25	5	-	25	4	+	1190655.400	0.11	619.52	579.80	25.12
0	25	5	+	25	4	-	1191077.097	-0.10	619.52	579.79	25.13
0	24	5	-	24	4	+	1191948.675	0.02	579.28	539.52	24.01
0	24	5	+	24	4	-	1192256.097	-0.09	579.28	539.51	24.01
0	23	5	-	23	4	+	1193087.616	-0.01	540.65	500.85	22.89
0	23	5	+	23	4	-	1193308.540	-0.06	540.65	500.84	22.90
0	22	5	-	22	4	+	1194085.816	-0.02	503.62	463.79	21.78
0	22	5	+	22	4	-	1194242.132	-0.03	503.62	463.78	21.78
0	21	5	-	21	4	+	1194956.058	0.02	468.19	428.33	20.67
0	21	5	+	21	4	-	1195064.783	0.00	468.19	428.32	20.68
0	20	5	-	20	4	+	1195710.239	0.01	434.36	394.48	19.57

which have been frequency- and phase-stabilized in Cologne up to 1.25 THz. The terahertz spectrometer has been described previously (*15, 16*). The methanol pressure in the absorption cell was maintained between 0.4 and 4 Pa (3–30 mTorr). To frequency- and phase-lock the BWOs, the 6th through 11th harmonics of a KVARZ synthesizer, operating in the region 78–118 GHz, were used. The typical uncertainty in line position for unblended lines is ≈50 kHz, with a statistical uncertainty of less than 10 kHz.

In Fig. 1, we present the head of the $^rQ_4$ branch of methanol in the A symmetry substate of the $v_t = 0$ level ($\Delta J = 0$; $J = 5–9$, $5 \leftarrow 4 = |K|$), located near the highest frequency presently achievable in Cologne with broadband tunable BWOs. Such frequencies can also be generated with the use of frequency multipliers. To achieve frequencies higher than about 1.1 THz with frequency- and phase-locking, however, considerable precautions must be taken to minimize the

TABLE II—*Continued*

v_t	J'	K'	P'	J"	K"	P"	Frequency (MHz)	Res. (MHz)	E_u (cm^{-1})	E_l (cm^{-1})	μ^2S
0	20	5	+	20	4	-	1195784.520	0.03	434.36	394.48	19.57
0	19	5	-	19	4	+	1196359.668	0.03	402.15	362.24	18.47
0	19	5	+	19	4	-	1196409.361	0.03	402.15	362.24	18.47
0	18	5	-	18	4	+	1196914.790	0.00	371.54	331.61	17.37
0	18	5	+	18	4	-	1196947.317	0.01	371.54	331.61	17.37
0	17	5	-	17	4	+	1197385.533	0.00	342.53	302.59	16.27
0	17	5	+	17	4	-	1197406.346	0.06	342.53	302.59	16.27
0	16	5	-	16	4	+	1197781.091	0.02	315.14	275.18	15.17
0	16	5	+	16	4	-	1197793.964	0.01	315.14	275.18	15.17
0	15	5	-	15	4	+	1198109.993	-0.04	289.35	249.39	14.07
0	15	5	+	15	4	-	1198117.798	0.02	289.35	249.39	14.07
0	14	5	-	14	4	+	1198380.249	-0.18	265.17	225.20	12.96
0	14	5	+	14	4	-	1198384.998	0.08	265.17	225.20	12.96
0	12	5	+	12	4	-	1198775.246	-0.88	221.64	181.66	10.72
0	12	5	-	12	4	+	1198775.246	0.44	221.64	181.66	10.72
0	11	5	+	11	4	-	1198912.349	-0.41	202.29	162.30	9.58
0	11	5	-	11	4	+	1198912.349	0.26	202.29	162.30	9.58
0	10	5	+	10	4	-	1199017.526	-0.23	184.56	144.56	8.41
0	10	5	-	10	4	+	1199017.526	0.08	184.56	144.56	8.41
0	9	5	+	9	4	-	1199096.232	-0.14	168.43	128.43	7.08
0	9	5	-	9	4	+	1199096.232	0.00	168.43	128.43	7.08
0	8	5	+	8	4	-	1199153.295	-0.07	153.92	113.92	5.90
0	8	5	-	8	4	+	1199153.295	-0.02	153.92	113.92	5.90
0	7	5	+	7	4	-	1199193.043	-0.05	141.01	101.01	4.65
0	7	5	-	7	4	+	1199193.043	-0.03	141.01	101.01	4.65
0	6	5	+	6	4	-	1199219.364	-0.01	129.72	89.72	3.29
0	6	5	-	6	4	+	1199219.364	-0.01	129.72	89.72	3.29
0	5	5	+	5	4	-	1199235.634	0.01	120.04	80.04	1.77
0	5	5	-	5	4	+	1199235.634	0.02	120.04	80.04	1.77

absorption caused by the moisture of the air. For recording the terahertz radiation, we have installed a magnetically tuned hot electron InSb bolometer, optimized for operation between 1 and 2 THz. Details of these new experimental improvements will be published elsewhere. Additional molecules studied at Cologne using THz techniques include HOOH, SO, SH, and others (*17–19*).

The extended IAM treatment most recently described by Anderson *et al.* (*9, 20*) has been utilized to analyze the data taken at Cologne. The Hamiltonian, consisting of rotational, torsional, and torsional–rotational terms, is diagonalized in a two-step procedure in which the torsional eigenfunctions are determined first and then multiplied by symmetric top functions for use as basis functions in the second diagonalization. Matrix elements off-diagonal in torsional state by up to two states are included. The final eigenstates are described by the quantum numbers v_t, J, $|K|$, and P for the torsional levels of A symmetry and the quantum numbers v_t, J, and K for torsional levels of E symmetry, where $v_t = 0, 1, 2, \cdots$ is the torsional quantum number, J is the total angular momentum, K is its projection on the a internal (prolate) axis, and P $(+/-)$ is the parity (*3*). Methanol has nonzero dipole components along its a and b axes; these components do not change during torsional motion so that the torsional symmetry levels of A and E symmetry are not connected. The selection rules for strong rotational transitions within a torsional state are $\Delta J = 0$, $\Delta|K| = 0, 1, + \leftrightarrow -$; $\Delta J = \pm 1$, $\Delta|K| = 0, 1, \pm \leftrightarrow \pm$ for A levels and $\Delta J = 0, \pm 1$, $\Delta K = 0, \pm 1$ for E levels. Although not included in our data set,

TABLE III

CH_3OH *E* Transitions

v_t	J'	K'	J"	K"	Frequency (MHz)	Res. (MHz)	E_u (cm^{-1})	E_l (cm^{-1})	μ^2S
2	12	-7	11	-7	577247.260	-0.01	879.08	859.83	6.17
2	12	-3	11	-3	577533.294	-0.04	761.38	742.12	8.80
2	12	-8	11	-8	577561.310	0.08	763.10	743.83	5.15
2	12	4	11	4	577609.984	0.04	741.20	721.94	8.35
2	12	5	11	5	577627.635	-0.57	712.67	693.40	7.75
2	12	1	11	1	577697.072	0.28	680.77	661.50	9.33
2	12	-6	11	-6	577702.277	0.27	728.22	708.95	7.05
2	12	7	11	7	577720.042	-0.02	736.07	716.80	6.21
2	12	-4	11	-4	577804.930	0.25	642.95	623.68	8.36
2	12	6	11	6	577811.850	0.50	610.66	591.39	7.05
2	12	0	11	0	577824.292	0.11	635.77	616.49	9.40
1	12	3	11	3	577841.034	0.02	415.20	395.93	8.79
2	12	-5	11	-5	577855.564	0.42	565.50	546.22	7.76
2	12	-2	11	-2	577973.917	0.54	573.63	554.35	9.15
0	12	0	11	0	578006.395	-0.25	134.30	115.02	9.38
2	12	2	11	2	578027.789	-0.18	532.76	513.48	9.13
2	12	-1	11	-1	578045.202	-0.39	495.09	475.81	9.33
1	12	-7	11	-7	578077.176	0.09	488.95	469.67	6.32
1	12	-6	11	-6	578284.900	0.09	468.15	448.86	6.83
1	12	-2	11	-2	578365.086	-0.07	378.54	359.25	9.16
1	12	4	11	4	578432.109	-0.28	377.71	358.41	8.28
1	12	-3	11	-3	578481.862	-0.09	349.37	330.07	8.77
1	12	0	11	0	578516.198	-0.18	334.04	314.74	9.41
1	12	1	11	1	578526.051	-0.17	327.71	308.42	9.33
1	12	2	11	2	578702.848	0.12	403.12	383.82	9.17
1	12	-4	11	-4	578740.843	-0.11	406.93	387.62	8.38
1	12	-1	11	-1	578751.681	-0.08	412.48	393.18	9.33
1	12	-5	11	-5	578791.384	0.00	504.75	485.44	7.74
0	12	-1	11	-1	579151.005	-0.27	129.19	109.87	9.34
1	12	5	11	5	579184.859	-0.39	423.47	404.15	7.81
0	12	-8	11	-8	579687.780	0.12	348.79	329.45	5.20
0	12	7	11	7	579851.579	-0.13	299.01	279.67	6.22
0	12	-7	11	-7	579864.615	0.22	306.24	286.90	6.21
0	12	6	11	6	579904.466	0.01	249.67	230.32	7.04
0	12	-6	11	-6	579965.018	0.39	256.74	237.39	7.08
0	12	5	11	5	579990.800	0.01	219.98	200.63	7.76
0	12	-5	11	-5	580033.013	0.03	211.60	192.25	7.77
0	12	-4	11	-4	580058.360	-0.19	186.51	167.16	8.34
0	12	4	11	4	580125.582	0.05	192.15	172.80	8.40
0	12	-3	11	-3	580162.759	-0.10	169.02	149.67	8.86
0	12	1	11	1	580368.617	-0.28	140.09	120.73	9.52
0	12	3	11	3	580442.320	0.06	158.62	139.26	8.83
0	12	2	11	2	580902.728	0.22	140.99	121.61	9.05
0	12	-2	11	-2	581091.717	-0.10	143.54	124.16	9.15
1	25	-7	25	-6	610689.378	0.02	885.05	864.68	13.91
1	24	-7	24	-6	612720.300	-0.03	845.03	824.59	13.81

[a] Remeasurement of line originally measured by Herbst *et al.* (*5*).

[b] Remeasurement of lines originally measured by Johnston *et al.* (*23*).

transitions involving changes in torsional state ($\Delta v_t \neq 0$) occur and are prominent in the far-infrared region. Intensities, calculated assuming that the torsional motion is one-dimensional, are accurate to a few percent at best.

III. ANALYSIS AND DISCUSSION

We have analyzed transitions belonging to 14 *Q* branches; these are listed in Table I. Selected transitions from two of these have been studied previously; the

TABLE III—*Continued*

v_t	J'	K'	J"	K"	Frequency (MHz)	Res. (MHz)	E_u (cm^{-1})	E_l (cm^{-1})	$\mu^2 S$
1	23	-7	23	-6	614534.697	-0.02	806.59	786.09	13.65
1	22	-7	22	-6	616144.240	-0.01	769.74	749.19	13.43
1	21	-7	21	-6	617561.290	0.02	734.49	713.89	13.14
1	20	-7	20	-6	618798.688	0.04	700.82	680.18	12.80
1	19	-7	19	-6	619869.614	0.04	668.75	648.07	12.38
1	18	-7	18	-6	620787.458	0.04	638.27	617.56	11.91
1	17	-7	17	-6	621565.618	0.02	609.39	588.65	11.36
1	16	-7	16	-6	622217.418	0.00	582.10	561.35	10.75
1	15	-7	15	-6	622755.939	-0.02	556.41	535.64	10.07
1	14	-7	14	-6	623193.913	-0.04	532.33	511.54	9.33
1	13	-7	13	-6	623543.613	-0.04	509.84	489.04	8.51
1	12	-7	12	-6	623816.771	-0.05	488.95	468.15	7.61
1	11	-7	11	-6	624024.495	-0.04	469.67	448.86	6.64
1	10	-7	10	-6	624177.212	-0.01	451.99	431.17	5.57
1	9	-7	9	-6	624284.554	0.00	435.92	415.09	4.41
1	8	-7	8	-6	624355.450	0.03	421.45	400.62	3.12
1	7	-7	7	-6	624397.943	0.07	408.58	387.76	1.67
2	18	3	18	2	733168.905	-0.06	706.59	682.13	3.16
2	17	3	17	2	733230.181	-0.10	677.69	653.23	3.00
2	16	3	16	2	733282.921	-0.11	650.39	625.93	2.83
2	15	3	15	2	733328.010	-0.05	624.69	600.23	2.66
2	14	3	14	2	733366.214	0.03	600.60	576.14	2.49
2	13	3	13	2	733398.283	0.11	578.11	553.65	2.31
2	12	3	12	2	733424.922	0.16	557.23	532.76	2.14
2	11	3	11	2	733446.839	0.20	537.95	513.48	1.96
2	10	3	10	2	733464.510	0.07	520.27	495.80	1.77
2	9	3	9	2	733478.935	0.18	504.20	479.73	1.59
2	8	3	8	2	733490.240	0.13	489.74	465.27	1.40
2	7	3	7	2	733499.062	0.06	476.88	452.41	1.20
2	6	3	6	2	733505.810	-0.03	465.63	441.16	1.00
2	5	3	5	2	733510.893	-0.12	455.98	431.52	0.79
2	4	3	4	2	733514.603	-0.23	447.95	423.48	0.57
2	3	3	3	2	733517.340	-0.24	441.52	417.05	0.32
0	13	-5	13	-4	752100.668	0.28	232.56	207.47	12.13
0	14	-5	14	-4	752106.629	0.29	255.13	230.04	13.28
0	12	-5	12	-4	752112.346	0.24	211.60	186.51	10.98
0	15	-5	15	-4	752134.297	0.24	279.30	254.22	14.42
0	11	-5	11	-4	752137.864	0.19	192.25	167.16	9.81
0	10	-5	10	-4	752173.658	0.08	174.51	149.42	8.62
0	16	-5	16	-4	752188.095	0.20	305.09	280.00	15.56
0	9	-5	9	-4	752216.520	-0.04	158.39	133.30	7.40
0	8	-5	8	-4	752263.501	-0.17	143.87	118.78	6.14
0	17	-5	17	-4	752272.597	0.11	332.49	307.40	16.70
0	7	-5	7	-4	752311.943	-0.32	130.97	105.88	4.81
0	6	-5	6	-4	752359.491	-0.46	119.68	94.59	3.39
0	18	-5	18	-4	752392.726	0.01	361.49	336.40	17.84
0	5	-5	5	-4	752404.080	-0.60	110.01	84.91	1.83
0	19	-5	19	-4	752553.621	-0.08	392.11	367.00	18.98
0	20	-5	20	-4	752760.641	-0.17	424.33	399.22	20.13

other transitions are all new. The Q-branch transitions, which belong to the three lowest torsional levels, were assigned by a combination of proximity to predicted frequencies, and loop and error-curve techniques (*9*). In addition to these Q-branch transitions, we have extended the previous *a*R-branch data by including transitions from the following three branches: $J = 12 \leftarrow 11$, $J = 18 \leftarrow 17$, and $J = 22 \leftarrow 21$. Predicted transition frequencies from fits to lower J data allowed tentative assignments to be made. Since the previous *a*R-branch data extended only to $J = 10 \leftarrow 9$, there was no universal way to confirm the new assignments except by their residuals in the current least-squares-fitting procedure. Experience

TABLE III—*Continued*

v_t	J'	K'	J"	K"	Frequency (MHz)	Res. (MHz)	E_u (cm^{-1})	E_l (cm^{-1})	μ^2S	
0	21	-5	21	-4	753019.382	-0.22	458.15	433.03	21.29	
0	22	-5	22	-4	753335.634	-0.21	493.58	468.45	22.45	
0	23	-5	23	-4	753715.367	-0.10	530.62	505.48	23.62	
0	17	-3	17	-2	753866.637	-0.21	289.93	264.78	15.39	
0	24	-5	24	-4	754164.684	0.13	569.26	544.11	24.81	
0	16	-3	16	-2	756799.911	-0.14	262.53	237.28	14.66	
0	15	-3	15	-2	759199.843	-0.10	236.74	211.41	13.86	
0	14	-3	14	-2	761136.175	-0.08	212.55	187.17	13.01	
0	13	-3	13	-2	762676.347	-0.08	189.98	164.54	12.12	
0	12	-3	12	-2	763882.843	-0.08	169.02	143.54	11.19	
0	11	-3	11	-2	764811.800	-0.08	149.67	124.16	10.24	
0	10	-3	10	-2	765512.621	-0.08	131.93	106.39	9.27	
0	9	-3	9	-2	766028.293	-0.06	115.80	90.24	8.28	
0	8	-3	8	-2	766395.950	-0.04	101.28	75.71	7.28	
0	7	-3	7	-2	766647.562	0.01	88.37	62.80	6.25	
0	6	-3	6	-2	766810.492	0.06	77.08	51.50	5.20	
0	5	-3	5	-2	766908.085	0.12	67.40	41.82	4.10	
0	4	-3	4	-2	766959.934	0.18	59.33	33.75	2.94	
0	3	-3	3	-2	766982.199	0.24	52.88	27.29	1.63	
0	25	5	25	4	829386.291	-0.17	617.72	590.06	21.89	
0	24	5	24	4	830087.623	-0.02	577.50	549.82	21.00	
0	23	5	23	4	830720.642	0.13	538.89	511.18	20.11	
0	22	5	22	4	831289.953	0.17	501.87	474.14	19.21	
0	21	5	21	4	831800.191	0.17	466.46	438.71	18.31	
0	20	5	20	4	832255.780	0.12	432.65	404.89	17.39	
0	19	5	19	4	832661.031	0.07	400.44	372.67	16.48	
0	18	5	18	4	833020.038	0.01	369.84	342.06	15.55	
0	17	5	17	4	833336.744	-0.05	340.85	313.05	14.62	
0	16	5	16	4	833614.888	-0.10	313.46	285.65	13.67	
0	15	5	15	4	833858.048	-0.13	287.68	259.86	12.72	
0	14	5	14	4	834069.562	-0.14	263.50	235.68	11.75	
0	13	5	13	4	834252.608	-0.14	240.94	213.11	10.77	
0	12	5	12	4	834410.145	-0.12	219.98	192.15	9.78	
0	11	5	11	4	834544.930	-0.08	200.63	172.80	8.76	
0	10	5	10	4	834659.510	-0.03	182.90	155.06	7.72	
0	9	5	9	4	834756.217	0.04	166.77	138.93	6.64	
0	8	5	8	4	834837.187	0.11	152.26	124.41	5.52	
0	7	5	7	4	834904.332	0.19	139.36	111.51	4.34	
0	6	5	6	4	834959.356	0.27	128.07	100.21	3.06	
0	5	5	5	4	835003.750	0.35	118.39	90.53	1.65	
1	25	-2	25	-3	866246.865	0.10	774.92	746.03	17.05	
1	24	-2	24	-3	867558.378	-0.05	734.86	705.92	16.80	
1	18	-5	17	-5	868069.932	0.11	654.36	625.40	12.97	
1	23	-2	23	-3	868720.489	0.23	696.39	667.42	16.50	
0	18	-8	17	-8	868804.124	-0.30	498.57	469.59	11.26	
0	18	8	17	8	868976.006	-0.01	508.10	479.12	11.34	
0	7	3	6	2	869037.910	0.22	77.95	48.96	6.29	a
0	18	-7	17	-7	869088.367	0.39	456.07	427.08	11.99	
0	18	7	17	7	869190.462	0.07	448.85	419.86	12.01	
0	18	6	17	6	869237.357	0.12	399.52	370.52	12.51	

has shown us that in a least-squares-fitting procedure with as many parameters as the present one, it is desirable to be able to confirm line assignments with the additional analyses used for the Q branches. We have therefore been cautious in assigning new ^aR-branch transitions; only those lines close to predicted frequencies have been included in the data set. To assign ^aR-branch data securely and more comprehensively, it will be necessary to use a bootstrap procedure in which the J quantum number is increased gradually. The same rationale has been utilized to exclude for the time being the very-high-frequency (>1.5 THz) high-resolution data from our fit (*1*, *11*). Xu and Hougen (*10*) have included some very-high-

TABLE III—*Continued*

v_t	J'	K'	J"	K"	Frequency (MHz)	Res. (MHz)	E_u (cm^{-1})	E_l (cm^{-1})	μ^2S	
0	18	5	17	5	869268.183	0.13	369.84	340.85	13.01	
0	18	-4	17	-4	869422.191	-0.03	336.40	307.40	13.39	
1	18	5	17	5	869450.228	-0.25	573.26	544.26	13.11	
0	18	-5	17	-5	869542.318	-0.13	361.49	332.49	13.01	
0	18	4	17	4	869584.888	0.07	342.06	313.05	13.47	
0	18	-3	17	-3	869603.224	-0.38	318.93	289.93	13.78	
1	22	-2	22	-3	869742.267	-0.32	659.52	630.50	16.15	
1	21	-2	21	-3	870634.504	-0.36	624.23	595.19	15.76	
1	20	-2	20	-3	871408.289	0.00	590.54	561.47	15.32	
1	19	-2	19	-3	872072.422	0.04	558.44	529.35	14.84	
1	18	-2	18	-3	872637.086	0.07	527.94	498.83	14.32	
1	17	-2	17	-3	873111.865	0.10	499.04	469.92	13.75	
1	16	-2	16	-3	873506.041	0.11	471.74	442.60	13.14	
1	15	-2	15	-3	873828.541	0.12	446.03	416.89	12.50	
1	14	-2	14	-3	874087.897	0.11	421.93	392.78	11.81	
1	13	-2	13	-3	874292.232	0.09	399.43	370.27	11.09	
1	12	-2	12	-3	874449.194	0.06	378.54	349.37	10.33	
1	11	-2	11	-3	874565.972	0.03	359.25	330.07	9.54	
1	10	-2	10	-3	874649.235	0.01	341.56	312.38	8.71	
1	9	-2	9	-3	874705.131	-0.03	325.48	296.30	7.85	
1	8	-2	8	-3	874739.273	-0.08	311.00	281.82	6.96	
1	3	-2	3	-3	874742.450	-0.09	262.74	233.56	1.60	
1	4	-2	4	-3	874751.813	-0.17	269.17	239.99	2.88	
1	7	-2	7	-3	874756.730	-0.15	298.13	268.95	6.02	
1	5	-2	5	-3	874759.394	-0.11	277.22	248.04	4.00	
0	19	6	19	5	889573.029	0.02	430.12	400.44	17.83	
0	18	6	18	5	889584.533	0.36	399.52	369.84	16.74	
0	20	6	20	5	889584.533	-0.42	462.32	432.65	18.92	
0	17	6	17	5	889615.012	0.02	370.52	340.85	15.64	
0	21	6	21	5	889623.640	0.02	496.13	466.46	20.01	
0	16	6	16	5	889662.233	0.02	343.13	313.46	14.53	
0	22	6	22	5	889692.827	0.02	531.55	501.87	21.09	
0	15	6	15	5	889722.746	0.03	317.35	287.68	13.41	
0	14	6	14	5	889793.596	-0.02	293.18	263.50	12.28	
0	23	6	23	5	889796.617	0.15	568.57	538.89	22.17	
0	13	6	13	5	889872.177	0.03	270.62	240.94	11.13	b
0	24	6	24	5	889938.728	0.01	607.19	577.50	23.25	
0	12	6	12	5	889955.805	0.03	249.67	219.98	9.96	b
0	11	6	11	5	890042.144	0.03	230.32	200.63	8.76	b
0	25	6	25	5	890123.832	-0.01	647.41	617.72	24.33	
0	10	6	10	5	890128.999	0.03	212.59	182.90	7.52	b
0	9	6	9	5	890214.362	0.02	196.47	166.77	6.24	b
0	8	6	8	5	890296.403	0.02	181.96	152.26	4.88	b
0	7	6	7	5	890373.473	0.01	169.06	139.36	3.42	b
0	6	6	6	5	890444.111	0.00	157.77	128.07	1.83	b
0	23	4	23	3	991849.987	-0.05	511.18	478.09	22.54	
0	22	4	22	3	994136.582	-0.03	474.14	440.98	21.52	
0	21	4	21	3	996146.335	0.02	438.71	405.49	20.49	
0	20	4	20	3	997899.637	0.05	404.89	371.60	19.45	
0	19	4	19	3	999417.045	0.05	372.67	339.33	18.42	

frequency data and shown that they are well fitted by the IAM procedure. We have included blended lines in the new data, especially *K* doublets belonging to the *A* torsional states. These lines have been weighted down, rather than removed as had been done previously (*9*).

In Tables II and III, we list our newly measured spectral lines for the *A* and *E* torsional states, respectively. In addition to quantum numbers and frequencies, the tables contain residuals (measured − calculated frequencies), upper and lower state energies (cm^{-1}), and intensities. The energies are reported with respect to the lowest level, the $v_t = 0$ *A* rotationless level. The intensities are reported as

TABLE III—*Continued*

v_t	J'	K'	J"	K"	Frequency (MHz)	Res. (MHz)	E_u (cm^{-1})	E_l (cm^{-1})	μ^2S
0	18	4	18	3	1000718.982	0.03	342.06	308.68	17.38
0	17	4	17	3	1001825.533	0.01	313.05	279.63	16.35
0	16	4	16	3	1002756.208	-0.03	285.65	252.20	15.31
0	15	4	15	3	1003529.861	-0.07	259.86	226.39	14.27
0	14	4	14	3	1004164.550	-0.10	235.68	202.18	13.22
0	13	4	13	3	1004677.413	-0.12	213.11	179.60	12.18
0	12	4	12	3	1005084.637	-0.12	192.15	158.62	11.12
0	11	4	11	3	1005401.387	-0.10	172.80	139.26	10.06
0	10	4	10	3	1005641.717	-0.07	155.06	121.51	8.99
0	9	4	9	3	1005818.570	-0.06	138.93	105.38	7.90
0	8	4	8	3	1005943.852	-0.02	124.41	90.86	6.79
0	7	4	7	3	1006028.222	0.05	111.51	77.95	5.64
0	6	4	6	3	1006081.187	0.11	100.21	66.65	4.44
0	5	4	5	3	1006111.077	0.18	90.53	56.97	3.15
0	4	4	4	3	1006125.054	0.24	82.47	48.91	1.72
1	2	-1	2	-2	1016092.494	0.02	291.80	257.91	0.41
1	3	-1	3	-2	1016113.978	0.02	296.63	262.74	0.72
1	4	-1	4	-2	1016147.850	0.02	303.07	269.17	1.00
1	5	-1	5	-2	1016198.575	0.03	311.11	277.22	1.27
1	6	-1	6	-2	1016271.730	0.02	320.77	286.87	1.54
1	7	-1	7	-2	1016374.015	0.02	332.03	298.13	1.80
1	8	-1	8	-2	1016513.294	0.08	344.91	311.00	2.07
1	9	-1	9	-2	1016698.254	0.01	359.39	325.48	2.33
1	10	-1	10	-2	1016939.065	0.00	375.48	341.56	2.60
1	11	-1	11	-2	1017246.714	-0.01	393.18	359.25	2.86
1	12	-1	12	-2	1017633.314	-0.02	412.48	378.54	3.13
1	13	-1	13	-2	1018112.000	-0.04	433.39	399.43	3.41
1	14	-1	14	-2	1018696.936	-0.05	455.91	421.93	3.68
1	15	-1	15	-2	1019403.266	-0.05	480.04	446.03	3.96
1	16	-1	16	-2	1020247.075	-0.06	505.77	471.74	4.24
1	17	-1	17	-2	1021245.388	-0.05	533.11	499.04	4.53
1	18	-1	18	-2	1022416.049	-0.03	562.05	527.94	4.82
1	19	-1	19	-2	1023777.726	-0.01	592.59	558.44	5.11
1	20	-1	20	-2	1025349.815	0.02	624.74	590.54	5.40
1	21	-1	21	-2	1027152.369	0.05	658.49	624.23	5.70
1	22	-1	22	-2	1029205.980	0.06	693.85	659.52	6.00
1	23	-1	23	-2	1031531.690	0.07	730.80	696.39	6.31
1	24	-1	24	-2	1034150.721	0.01	769.36	734.86	6.62
1	25	-1	25	-2	1037084.211	-0.13	809.52	774.92	6.92
0	22	8	21	8	1061334.020	-0.37	640.09	604.69	14.99
0	22	-7	21	-7	1061448.488	0.33	588.08	552.67	15.51
0	22	7	21	7	1061705.477	0.22	580.88	545.47	15.54
0	22	6	21	6	1061727.826	0.09	531.55	496.13	15.91
0	22	-4	21	-4	1061905.528	-0.25	468.45	433.03	16.64
0	22	4	21	4	1062168.878	0.09	474.14	438.71	16.74
0	22	-5	21	-5	1062221.787	-0.24	493.58	458.15	16.33
0	22	2	21	2	1062312.217	-0.08	423.27	387.84	17.01

the product of the component of the dipole moment squared [D^2; $\mu_a = 0.89$ D, $\mu_b = -1.44$ D (*21*)] and the S value (*22*). More accurate dipole moment values as a function of torsional state are known (*21*). Containing transitions with $J \leq 25$ and $|K| \leq 8$, the new data have been added to the previously measured lines of Anderson *et al.* (*9*) to form a global data set consisting of 790 A lines and 753 E lines under 1.2 THz in frequency.

The global data set has been analyzed with the extended IAM approach of De Lucia and co-workers (*6*, *9*) in which the A and E lines are treated separately. The A lines have been fit with a variance of 100 kHz by varying 62 parameters while the E lines have been fit with a variance of 150 kHz by varying 71 parameters. The numbers of parameters used are not significantly larger than in the

TABLE IV

New Spectroscopic Constants of CH_3OH[a]

Constant[b] (MHz unless noted)	Operator	A Species	E Species
A	P_a^2	127538.1491(0.06)	127491.02595(1.)
B	P_b^2	24692.07763(0.06)	24691.22501(0.1)
C	P_c^2	23758.00111(0.05)	23758.78906(0.1)
D_{ab}	$\{P_a,P_b\}$[c]	55.107093(0.4)	-115.793474(0.2)
F (cm^{-1}) x 10^3	P_γ^2 [d]	27646.29233(0.02)	27651.553364(0.6)
ρ (unitless) x 10^4	-- [d]	8096.623984(0.0006)	8097.097243(0.02)
V_3 (cm^{-1})	(1/2)(1-cos3γ)	373.352522(0.0004)	373.883355(0.03)
V_6 (cm^{-1})	(1/2)(1-cos6γ)	-0.8(fixed)	-2.075765(0.06)
F_v	P^2(1-cos3γ)	-71.520470(0.002)	-71.567292(0.004)
G_v	$P^2P_\gamma^2$	-3.546278(0.0003)	-3.559332(0.0006)
L_v x 10^2	$P^2P_aP_\gamma$	7.516925(0.03)	5.776801(0.06)
Δ_{JK} x 10^2	$-P^2P_a^2$	19.322501(0.04)	28.389568(0.03)
Δ_J x 10^3	$-P^4$	50.66897(0.004)	50.66868(0.02)
Δ_K x 10	$-P_a^4$	4.6620892(0.02)	13.737988(0.1)
k_1	$P_a^3P_\gamma$	0.0(fixed)	-7.839480 (0.6)
k_2	$P_a^2P_\gamma^2$	-68.405566 (0.006)	-56.395754 (0.4)
k_3	$P_aP_\gamma^3$	-169.720076(0.006)	-157.038989(2.)
k_4	P_γ^4	-292.314360(0.03)	-218.59466(3.)
k_5	P_a^2(1-cos3γ)	304.26808(0.08)	406.18305(4.)
k_6	$\{P_aP_\gamma,$(1-cos3γ)$\}$	884.0(fixed)	884.0(fixed)
δ_J x 10^3	$-2P^2(P_b^2-P_c^2)$	1.76248(0.05)	2.740162(0.08)
δ_K x 10^2	$-\{P_a^2,(P_b^2-P_c^2)\}$	-18.529671(0.4)	8.2027394(0.7)
c_1	$\{(P_b^2-P_c^2),P_\gamma^2\}$	-1.8554459(0.005)	-1.6474041(0.01)
c_2	$(P_b^2-P_c^2)$(1-cos3γ)	-3.804494(0.05)	-1.503317(0.1)
H_J x 10^6	P^6	0.0(fixed)	-0.0252(0.01)
H_{JK} x 10^4	$P^4P_a^2$	0.135981(0.01)	0.032572(0.004)
H_{KJ} x 10^4	$P^2P_a^4$	0.503221(0.01)	0.246732(0.05)
H_K x 10^4	P_a^6	-115.4215(0.4)	3.303098(1.)
h_J x 10^6	$P^4(P_b^2-P_c^2)$	0.2717(0.02)	0.1463(0.05)
h_{JK} x 10^4	$P^2\{P_a^2,(P_b^2-P_c^2)\}$	0.300884(0.02)	0.0(fixed)
f_v x 10^4	P^4(1-cos3γ)	0.426792(0.09)	0.0(fixed)

[a] Figures in parentheses represent 1σ deviations. The number of listed significant figures for each constant is necessary to reproduce calculated frequencies to 10 kHz.

[b] The constants l_{JKK1}, l_{JKK2}, and the last four on the list are named using the notation of reference *(9)*. The constant h_{JK6} refers to the expansion of the centrifugal distortion parameter h_{JK}.

[c] $\{A,B\} = AB + BA$.

[d] P_γ refers to the torsional angular momentum + ρP_a - see references*(5)* and *(9)*.

previous fit of Anderson *et al.* to a much smaller data set, in which 57 and 64 parameters were varied for the *A* and *E* data, respectively (*9*). The spectroscopic parameters determined by the current approach and their corresponding operators are listed in Table IV with 1σ uncertainties. In general, the low-order constants are not changed dramatically from those of the previous fits but the higher-order constants change considerably. The terminology for the many interaction constants is taken from the notation of Anderson *et al.* (*9*). The fit to the data

TABLE IV—*Continued*

Constant [b] (MHz unless noted)	Operator	A Species	E Species
$c_3 \times 10^2$	$\{(P_b^2-P_c^2),P_\gamma^4\}$	3.694848(0.04)	-1.3513421(0.2)
c_4	$\{P_aP_\gamma,(P_b^2-P_c^2)\}$	-0.444467 (0.01)	-1.168516(0.05)
d_{ab}	$\{P_a,P_b\}(1-\cos3\gamma)$	0.0(fixed)	280.13274(0.3)
Δ_{ab}	$\{\{P_a,P_b\},P_\gamma^2\}$	-37.095169(0.1)	-15.216942(0.03)
δ_{ab}	$\{\{P_a,P_b\},P_aP_\gamma\}$	-5.6468165(0.05)	0.2178952(0.06)
$g_v \times 10^4$	$P^4P_\gamma^2$	0.540532(0.008)	0.0(fixed)
$l_v \times 10^4$	$P^4P_aP_\gamma$	-0.315907 (0.01)	0.0(fixed)
$\phi_v \times 10^2$	$P^2P_a^2(1-\cos3\gamma)$	11.75595(0.04)	1.085084(0.04)
$\gamma_v \times 10^2$	$P^2P_a^2P_\gamma^2$	0.8320866(0.003)	0.6220534(0.01)
$\lambda_v \times 10^2$	$P^2P_a^3P_\gamma$	0.3866909(0.004)	-0.1525097(0.007)
$c_6 \times 10^4$	$-2P^2(P_b^2-P_c^2)(1-\cos3\gamma)$	-3.318234(0.3)	9.837626(0.6)
$c_5 \times 10^4$	$\{-2P^2(P_b^2-P_c^2),P_\gamma^2\}$	4.018473(0.04)	2.019604(0.1)
$c_7 \times 10^4$	$\{-2P^2(P_b^2-P_c^2),P_aP_\gamma\}$	-0.704629(0.06)	0.559733(0.06)
$c_9 \times 10^2$	$-\{P_a^2,(P_b^2-P_c^2)\}(1-\cos3\gamma)$	-1.095327(0.5)	7.648913(0.4)
$c_8 \times 10^2$	$-\{\{P_a^2,(P_b^2-P_c^2)\},P_\gamma^2\}$	-0.435699(0.02)	-1.012009(0.05)
$c_{10} \times 10^4$	$-\{\{P_a^2,(P_b^2-P_c^2)\},P_aP_\gamma\}$	0.0(fixed)	-18.916820(1.)
$\Delta\Delta_{ab}$	$\{\{P_a,P_b\},P_\gamma^4\}$	0.934104(0.007)	0.0(fixed)
$\delta\delta_{ab} \times 10^2$	$\{\{P_a,P_b\},P_aP_\gamma^3\}$	32.8374(0.2)	3.738176(0.6)
$h_{K1} \times 10^4$	$P^2P_a^4(1-\cos3\gamma)$	0.0 (fixed)	-3.61316(0.2)
$h_{K2} \times 10^4$	$P^2P_a^4P_\gamma^2$	0.0 (fixed)	0.448512(0.05)
$h_{K3} \times 10^4$	$P^2P_a^5P_\gamma$	-0.38923(0.007)	0.263628(0.01)
$h_{J1} \times 10^4$	$P^4P_a^2(1-\cos3\gamma)$	0.150451(0.01)	0.0(fixed)
$h_{J2} \times 10^6$	$P^4P_a^2P_\gamma^2$	-0.3562(0.1)	0.0(fixed)
$d\delta_{ab} \times 10^2$	$\{\{P_a,P_b\},P_a^2P_\gamma^2\}$	0.0(fixed)	11.944841(0.3)
$\delta d_{ab} \times 10$	$\{\{P_a,P_b\},P_a^3P_\gamma\}$	-0.516770(0.003)	0.0(fixed)
$N_v \times 10^2$	$P^2(1-\cos6\gamma)$	-22.480896(0.3)	-14.9119652(0.5)
$Q_v \times 10^4$	$P^2P_aP_\gamma^3$	0.0(fixed)	17.26380(0.6)
$K_1 \times 10$	$P_a^2P_\gamma^4$	0.0(fixed)	-6.55860(0.8)
K_3	$P_a^3P_\gamma^3$	0.0(fixed)	-2.67303(0.3)
c_{11}	$(P_b^2-P_c^2)(1-\cos6\gamma)$	-3.2066613(0.04)	0.0(fixed)
$c_{12} \times 10^2$	$\{(P_b^2-P_c^2),P_aP_\gamma^3\}$	-4.841220(0.1)	-1.801748(0.3)

allows us to predict the frequencies and intensities for large numbers of transitions through $J = 25$ and 1.2 THz in frequency, which were not measured in the laboratory. The predictions as well as the global data set are available electronically from the authors and supersede the previous predictions available through 1 THz.

ACKNOWLEDGMENTS

We thank Thomas Klaus for help with the experimental details. E.H. acknowledges the support of NASA for the Ohio State program in laboratory astrophysics. E.H. and G.W. thank the Max-Planck-Gesellschaft and the Alexander-von-Humboldt-Stiftung for the Max Planck Research Award. The spectral analysis was made possible by time awarded on the Cray YMP-8 computer of the Ohio Supercomputer Center. The work in Cologne was supported in part by the Deutsche Forschungsgemeinschaft (DFG) via Grant SFB

TABLE IV—*Continued*

Constant [b] (MHz unless noted)	Operator	A Species	E Species
$M_v \times 10^3$	$P^2P_\gamma^4$	1.41622(0.02)	2.419738(0.03)
$\mu_v \times 10^3$	$P^2P_a^2P_\gamma^4$	-0.783041(0.002)	-0.316166(0.006)
$\nu_v \times 10^2$	$P^2P_a^2(1-\cos 6\gamma)$	-17.387436(0.07)	-1.668673(0.03)
$\theta_v \times 10^4$	$P^2P_a^3P_\gamma^3$	-1.505754(0.01)	1.118315(0.06)
$g_k \times 10^2$	$P_a^4P_\gamma^2$	0.0(fixed)	7.461867(0.7)
$l_k \times 10^2$	$P_a^5P_\gamma$	0.0(fixed)	15.636728(1.)
$o_k \times 10^2$	$P_a^5P_\gamma^3$	0.0(fixed)	4.585342(0.5)
$h_{K4} \times 10^6$	$P^2P_a^4P_\gamma^4$	0.0(fixed)	1.0792(0.2)
$h_{K6} \times 10^6$	$P^2P_a^5P_\gamma^3$	0.0(fixed)	-2.2877(0.1)
$l_{JK2} \times 10^8$	$P^4P_a^4P_\gamma^2$	0.0(fixed)	-0.54(0.1)
$L_{JK} \times 10^6$	$P^4P_a^4$	-0.0506(0.003)	0.0(fixed)
$L_K \times 10^6$	P_a^8	0.0(fixed)	24.0083(4.)
$L_{JJK} \times 10^8$	$P^6P_a^2$	0.0(fixed)	0.26(0.04)
$l_{JKK1} \times 10^6$	$P^2P_a^6(1-\cos 3\gamma)$	0.0(fixed)	4.4518(0.3)
$l_{JKK2} \times 10^6$	$P^2P_a^6P_\gamma^2$	0.0(fixed)	-0.7597(0.05)
$c_{13} \times 10^3$	$-2P^2(P_b^2-P_c^2)(1-\cos 6\gamma)$	-1.13372(0.05)	-3.73967(0.1)
$c_{14} \times 10^6$	$\{-2P^2(P_b^2-P_c^2),P_\gamma^4\}$	-14.8136(0.4)	9.0216(2.)
$c_{15} \times 10^6$	$\{-2P^2(P_b^2-P_c^2),P_aP_\gamma^3\}$	-11.2045(0.6)	16.1202(2.)
$c_{16} \times 10^2$	$-\{P_a^2,(P_b^2-P_c^2)\}(1-\cos 6\gamma)$	26.15666(0.7)	0.0(fixed)
$c_{17} \times 10^4$	$-\{\{P_a^2,(P_b^2-P_c^2)\},P_\gamma^4\}$	0.0(fixed)	8.0739(0.4)
$h_{J5} \times 10^6$	$P^4P_a^2(1-\cos 6\gamma)$	-16.4977(2.)	0.0(fixed)
$h_{J4} \times 10^8$	$P^4P_a^2P_\gamma^4$	-4.69(0.7)	0.0(fixed)
$h_{J6} \times 10^8$	$P^4P_a^3P_\gamma^3$	5.05(0.3)	0.0(fixed)
$h_{JK6} \times 10^8$	$P^2\{\{P_a^2,(P_b^2-P_c^2)\},P_aP_\gamma^3\}$	0.0(fixed)	68.60(3.)

301 and special funding from the Science Ministry of the Land Nordrhein-Westfalen. The work of S.P.B. at Cologne was made possible by the DFG through grants aimed at supporting Eastern and Central European countries and the republics of the former Soviet Union.

REFERENCES

1. G. Moruzzi, B. P. Winnewisser, M. Winnewisser, I. Mukhopadhyay, and F. Strumia, "Microwave, Infrared, and Laser Transitions of Methanol: Atlas of Assigned Lines from 0 to 1258 cm^{-1}," CRC Press, Orlando, 1995, in press.
2. G. A. Blake, E. C. Sutton, C. R. Masson, and T. G. Phillips, *Astrophys. J.* **315,** 621–645 (1987).
3. R. M. Lees and J. G. Baker, *J. Chem. Phys.* **48,** 5299–5318 (1968).
4. J. S. Kochler and D. M. Dennison, *Phys. Rev.* **57,** 1006–1021 (1940).
5. E. Herbst, J. K. Messer, F. C. De Lucia, and P. Helminger, *J. Mol. Spectrosc.* **108,** 42–57 (1984).
6. F. C. De Lucia, E. Herbst, T. Anderson, and P. Helminger, *J. Mol. Spectrosc.* **134,** 395–411 (1989).
7. H. M. Pickett, E. A. Cohen, D. E. Brinza, and M. M. Schaefer, *J. Mol. Spectrosc.* **89,** 542–547 (1981).
8. G. Moruzzi, F. Strumia, J. C. S. Moraes, R. M. Lees, I. Mukhopadhyay, J. W. C. Johns, B. P. Winnewisser, and M. Winnewisser, *J. Mol. Spectrosc.* **153,** 511–577 (1992).
9. T. Anderson, E. Herbst, and F. C. De Lucia, *Astrophys. J. Suppl. Ser.* **82,** 405–444 (1992).
10. L-H. Xu and J. T. Hougen, *J. Mol. Spectrosc.* **169,** 396–409 (1995).

11. F. MATSUSHIMA, K. M. EVENSON, AND L. R. ZINK, *J. Mol. Spectrosc.* **164,** 517–530 (1994).
12. L-H. XU AND J. T. HOUGEN, *J. Mol. Spectrosc.*, in press.
13. S. TSUNEKAWA, T. UKAI, A. TOYAMA, AND K. TAKAGI, to be published.
14. J. TANG AND K. TAKAGI, *J. Mol. Spectrosc.* **161,** 487–498 (1993).
15. G. WINNEWISSER, A. F. KRUPNOV, M. YU. TRETYAKOV, M. LIEDTKE, F. LEWEN, A. H. SALECK, R. SCHIEDER, A. P. SHKAEV, AND S. V. VOLOKHOV, *J. Mol. Spectrosc.* **165,** 294–300 (1994).
16. G. WINNEWISSER, *Vib. Spectrosc.* **8,** 241–253 (1995).
17. A. F. KRUPNOV, S. P. BELOV, G. WINNEWISSER, J. BEHREND, M. LIEDTKE, R. SCHIEDER, K. M. T. YAMADA, AND E. HERBST, *Z. Naturforsch. A* **49,** 525–529 (1994).
18. TH. KLAUS, S. P. BELOV, A. H. SALECK, G. WINNEWISSER, AND E. HERBST, *J. Mol. Spectrosc.* **168,** 235–247 (1994).
19. E. KLISCH, TH. KLAUS, S. P. BELOV, G. WINNEWISSER, AND E. HERBST, in preparation.
20. T. ANDERSON, E. HERBST, AND F. C. DE LUCIA, *J. Mol. Spectrosc.* **159,** 410–421 (1993).
21. K. V. L. N. SASTRY, R. M. LEES, AND J. VAN DER LINDE, *J. Mol. Spectrosc.* **88,** 228–230 (1981).
22. C. H. TOWNES AND A. L. SCHAWLOW, "Microwave Spectroscopy," Dover, New York, 1975.
23. L. H. JOHNSTON, P. R. SRIVASTAWA, AND R. M. LEES, *J. Mol. Spectrosc.* **84,** 1–40 (1980).